

Research on Optimization and Control of Low-Temperature Cold Start Preheating of Proton Exchange Membrane Fuel Cell

Xiaopeng Li, Binbin Sun, Hailan Zhao, Huibin Liu

Abstract—Researching and improving the low-temperature cold-start performance of PEMFC plays an important role in the promotion and application of PEMFC. Among them, auxiliary preheating is one of the key technologies to achieve fast cold start of PEMFC. In order to reveal the influence law of auxiliary preheating parameters on the cold start of PEMFC, the auxiliary preheating control strategy is proposed. In this paper, a mathematical model for PEMFC performance analysis is first established. On this basis, the influence law of preheating exhaust gas temperature and flow rate on PEMFC temperature rise process is studied. Based on the Screening optimization algorithm, the input and output parameters of the preheating process were optimized, and the optimal auxiliary preheating control parameters were determined under different starting temperatures. Finally, a start-up auxiliary preheating control strategy for different low-temperature environments is designed and performance verification is carried out. The results show that the auxiliary preheating control strategy proposed in this paper reduces the start-up time by 43% at $-10\text{ }^{\circ}\text{C}$ compared without the auxiliary preheating control. The auxiliary strategy designed in this paper is able to achieve normal startup of the PEMFC at $-20\text{ }^{\circ}\text{C}$ and $-30\text{ }^{\circ}\text{C}$. However, the PEMFC startup fails in both without the auxiliary modes.

Index Terms—PEMFC, Low Temperature Cold Start, Auxiliary Preheating Control, Performance Optimization

I. INTRODUCTION

Researching and promoting hydrogen energy scenarios is important for reducing carbon emissions and achieving carbon neutrality [1,2]. The PEMFC has an important application potential in the automotive sector due to its

Manuscript received September 18, 2023; revised May 15, 2024. This work was supported in part by the Major Innovation Projects in Shandong under Grant 2020CXGC010405 and 2020CXGC010406, the Innovation team project of "Qing-Chuang science and technology plan" of colleges and universities in Shandong Province 2021KJ083, the National Natural Science Foundation Project of China under Grant 52102465, the Postdoctoral Science Foundation of China and Shandong under Grant 2020M680091 and 202003042.

Xiaopeng Li is a graduate student of School of Transportation and Vehicle Engineering, Shandong University of Technology, Zibo, 255000 PR China (e-mail: xiaopengli200105@163.com).

Binbin Sun is a Professor of School of Transportation and Vehicle Engineering, Shandong University of Technology, Zibo, 255000 PR China (corresponding author to provide phone: 86-13708941464; e-mail: sunbin_sdut@126.com).

Hailan Zhao is a teacher of Zibo Vocational Institute, Zibo, 255300 PR China (e-mail: 13708941464@126.com).

Huibin Liu is a postgraduate student in the School of Transportation and Vehicle Engineering, Shandong University of Technology, Zibo, 255000 PR China (e-mail: 1622763935@qq.com).

advantages of moderate operating temperature, high energy density and high specific power [3,4]. Due to the complexity of automotive application scenarios, there is a risk that without cold start control of the PEMFC in a low temperature environment, the PEMFC may not be able to start and operate properly [5]. Therefore, it is important to study and optimise the low-temperature cold start performance of PEMFC.

In the latest low temperature startup targets issued by the US Department of Energy, the lower temperature limit for successful startup without auxiliary measures is $-30\text{ }^{\circ}\text{C}$, and the lower temperature limit for startup with auxiliary measures is $-40\text{ }^{\circ}\text{C}$, and the requirement is to reach 50% of output power within 30s [6]. The national standard GBT33979-2017 Test Method for Low Temperature Characteristics of Proton Exchange Membrane Fuel Cell Power Generation System redefines the low-temperature cold start process. The process by which a fuel cell system is able to reach 90 per cent of its rated power output from a sub-zero temperature [7].

In order to improve the low-temperature cold start capability of the PEMFC, measures cited at the system level include purge after stopping the machine, reactive gas preheating, coolant heating, and an external miniature hydrogen catalytic burner [8,9]. Currently, PEMFCs can be classified into two types of startup based on whether or not auxiliary preheating is required, namely unassisted startup without any external energy and assisted startup with the help of external energy [10]. Unassisted startup means that the PEMFC relies on the heat generated by its own electrochemical reaction to increase its temperature, and assisted startup means that the PEMFC requires heat from an external heat source or an assisted reaction [11]. In this case, unassisted startup is limited by its own heat source resulting in a restricted minimum operating temperature [12].

In order to reveal the influence law of auxiliary preheating parameters on the cold start of PEMFC, the auxiliary preheating control strategy is proposed. In this paper, firstly, a mathematical model for PEMFC performance analysis was established. On this basis, the influence law of preheating exhaust gas temperature and flow rate on the temperature rise process of PEMFC is investigated. Further, the input and output parameters of the preheating process were optimised and analysed, and the optimal auxiliary preheating control parameters were determined for different start-up temperatures. Finally, the start-up auxiliary preheating control strategy is designed for different low temperature environments and performance is verified.

II. PEMFC NUMERICAL MODELLING

A. PEMFC output performance modelling

The actual output voltage of the PEMFC is calculated from four main components: reversible voltage, activation voltage drop, concentration difference voltage drop, and ohmic voltage drop. Among them, the activation voltage drop represents the loss caused by the activation of cell reactants. The concentration difference voltage drop represents the loss caused by the rapid consumption of battery reactants. The ohmic voltage drop represents the loss caused by the resistance of the battery components.

$$V = E_r - V_{act} - V_{ohm} - V_{con} \quad (1)$$

In the formula, V is the actual PEMFC voltage, E_r is the reversible voltage in the non-standard state, V_{act} is the activation voltage drop, V_{ohm} is the ohmic voltage drop, V_{con} is the concentration voltage drop.

B. Modelling of current density and electrochemical reaction rate

The current can be expressed in terms of the rate of redox reaction at the surface of the PEMFC electrode.

$$j = nFdN / dt \quad (2)$$

In the formula, j is the current, n is the number of electrons transferred per mole of hydrogen or oxygen during the reaction, dN / dt is the rate of consumption of the reactants of the electrochemical reaction, and F is the Faraday coefficient.

In order to facilitate the evaluation of the output performance of different cells, it can be measured by the output current per unit area, i.e. current density. In addition, it can be used to describe the electrochemical reaction rates.

$$J = \frac{j}{A} \quad (3)$$

In the formula, J is the current density, A is the PEMFC activation area.

C. Butler-Volmer equation

The current densities at the anode and cathode can be calculated from the Butler-Volmer equation.

$$J_a = J_a^{ref} \left(\frac{C_{H_2}}{C_{H_2}^{ref}} \right)^{s_a} \left(e^{\frac{Fa_a \eta_a}{RT}} - e^{-\frac{Fa_c \eta_c}{RT}} \right) \quad (4)$$

$$J_c = J_c^{ref} \left(\frac{C_{O_2}}{C_{O_2}^{ref}} \right)^{s_c} \left(-e^{\frac{Fa_a \eta_c}{RT}} + e^{-\frac{Fa_c \eta_c}{RT}} \right) \quad (5)$$

In the formula, J_a^{ref} is the anode reference exchange current density, J_c^{ref} is the cathode reference exchange current density, $C_{H_2}^{ref}$ is the hydrogen reference concentration,

$C_{O_2}^{ref}$ is the oxygen reference concentration, F is the Faraday coefficient, a is the transmission coefficient, s is the concentration coefficient, R is the universal gas constant, T is the temperature, and η is the activation overpotential.

D. Mass conservation equation

The gas mass conservation equation has a wide range of applications and it can be expressed as follows.

$$\frac{\partial(\varepsilon \rho_g (1 - v_{lq} - v_{ice}))}{\partial t} + \nabla \cdot (\rho_g \vec{u}_g) = S_m \quad (6)$$

In the formula, ε is the porosity of the porous medium, ρ_g is the gas density, \vec{u}_g is the gas velocity, v_{lq} is the liquid water volume fraction, v_{ice} is the ice volume fraction, and S_m is the mass source term.

This equation is used for the computational solution of the flow channel, the diffusion layer and the catalytic layer region.

E. Equation of conservation of momentum

The solution of the momentum conservation equation mainly involves the flow channel, the diffusion layer and catalytic layer region and is pushed to the following.

$$\frac{\partial}{\partial t} \left(\frac{\rho_g \vec{u}_g}{\varepsilon(1 - v_{lq} - v_{ice})} \right) = \mu_g \nabla \cdot \left\{ \nabla \left(\frac{\vec{u}_g}{\varepsilon(1 - v_{lq} - v_{ice})} \right) + \nabla \left(\frac{\vec{u}_g}{\varepsilon(1 - v_{lq} - v_{ice})} \right)^T \right\} - \nabla p_g - \nabla \cdot \left(\frac{\rho_g \vec{u}_g \vec{u}_g}{[\varepsilon(1 - v_{lq} - v_{ice})]^2} \right) - \frac{2}{3} \mu_g \nabla \cdot \left[\nabla \left(\frac{\vec{u}_g}{\varepsilon(1 - v_{lq} - v_{ice})} \right) \right] + S_u \quad (7)$$

In the formula, μ_g is the gas viscosity, P_g is the gas pressure, ε is the porosity of the porous medium, and S_u is the momentum source term, which is used in the computational solution of the flow channel, diffusion layer and catalytic layer region.

Among them, S_u is zero in the flow channel and can be expressed by Darcy's law in the porous medium region of the diffusion layer and the catalytic layer.

$$S_u = - \frac{\mu_g \vec{u}_g}{K_g} \quad (8)$$

In the formula, K_g is the gas permeability coefficient.

F. Energy Conservation Equation

The energy change during low temperature start-up of PEMFC involves various regions. Therefore, calculations need to be made for each region and the basic equations of energy conservation involved are as follows.

$$\frac{\partial((\rho C_p)_{fl,sl}^{eff} T)}{\partial t} = \nabla \cdot (k_{fl,sl}^{eff} \nabla T) - \nabla \cdot [T \vec{u}_g (\rho C_p)_{fl}^{eff}] + S_T \quad (9)$$

In the formula, $(\rho C_p)_{fl,sl}^{eff}$ is the effective volumetric heat capacity, $k_{fl,sl}^{eff}$ is the effective thermal conductivity, C_p is the specific heat capacity, S_T is the energy source item.

G. Component conservation equation

The solution of the component conservation equation mainly involves the flow channel, diffusion layer and catalytic layer regions, which are derived as follows.

$$\frac{\partial(\epsilon \rho_g Y_i (1 - v_{lq} - v_{ice}))}{\partial t} + \nabla \cdot (\rho_g \vec{u}_g Y_i) = \nabla \cdot (\rho_g D_i^{eff} \nabla Y_i) + S_i \quad (10)$$

In the formula, Y_i is the mass fraction of component i , D_i^{eff} is the effective diffusion coefficient of substance i , and S_i is the component source term, which is used to describe the transport of hydrogen, oxygen and water vapour.

Among them, the effective diffusion coefficient for water vapour is shown below.

$$D_{vp}^{eff} = \begin{cases} 1.055 \times 10^{-4} (P_{atm} / P)(T / 333)^{1.5} & \text{Anode} \\ 2.982 \times 10^{-5} (P_{atm} / P)(T / 333)^{1.5} & \text{Cathode} \end{cases} \quad (11)$$

In the formula, P_{atm} is the standard atmospheric pressure.

The effective diffusion coefficients of oxygen and hydrogen can be derived by the following equation.

$$D_{O_2}^{eff} = 2.652 \times 10^{-5} (P_{atm} / P)(T / 333)^{1.5} \quad (12)$$

$$D_{H_2}^{eff} = 1.055 \times 10^{-4} (P_{atm} / P)(T / 333)^{1.5} \quad (13)$$

III. PARAMETER OPTIMIZATION FOR OPTIMAL AUXILIARY HEATER OPERATION IN PROTON EXCHANGE MEMBRANE FUEL CELLS

In this paper, the difference between the preheating PEMFC temperature and the standard temperature is used as the output judgment parameter. The specified constraint is that, after satisfying the PEMFC temperature is not less than 0 °C, the minimum temperature difference is sought, and then the optimal preheating exhaust gas temperature and flow rate are determined. The optimization process is shown in Figure 1.

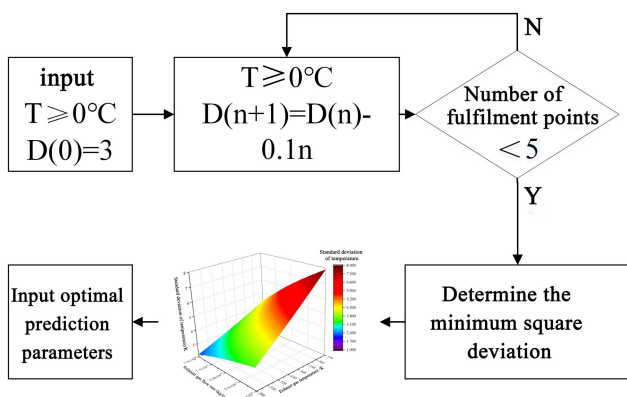
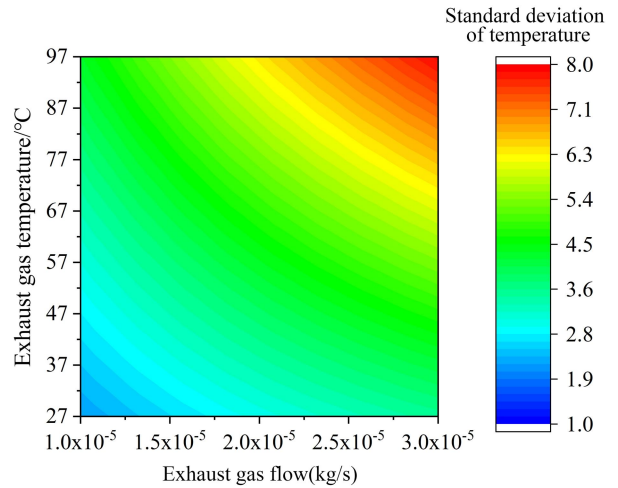
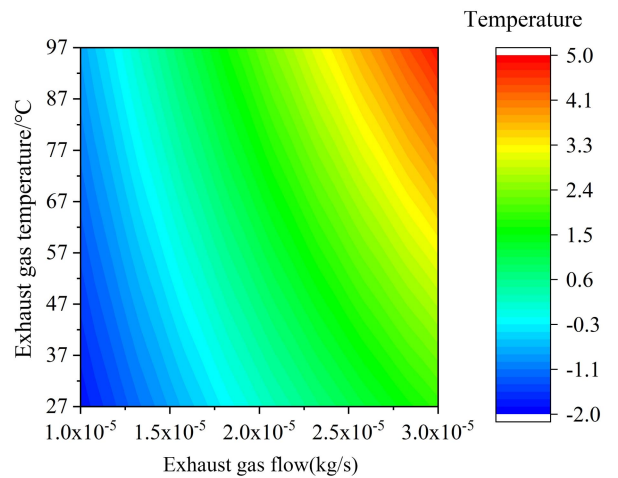


Fig. 1. Flow chart for determining optimal preheating operating parameters

Firstly, the input parameters and output parameters under -30 °C are optimized by the Screening optimization algorithm. The algorithm can filter and sort from 2000 samples, and supports input parameters for multiple target and constraint types. The boundary condition exhaust flow rate was set from 1×10^{-5} kg/s to 3×10^{-5} kg/s. The exhaust gas temperature was set from 27 °C to 97 °C. The warm-up time is set to 50 s. As shown in Figure 2 that there are the preheating exhaust gas temperature and flow rate, and PEMFC standard temperature difference and temperature in Z-axis projection map plot.



(a) The standard deviation map of exhaust gas temperature and flow rate and PEMFC temperature

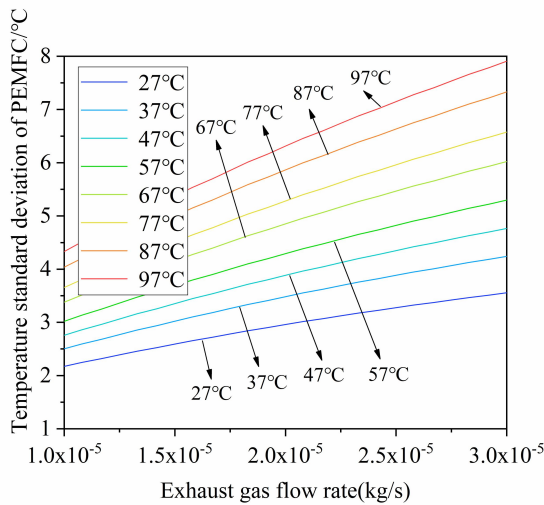


(b) Exhaust gas temperature and flow rate map with PEMFC temperature
Fig. 2. The standard deviation between -30 °C input parameters and PEMFC temperature and the temperature are projected on the Z-axis

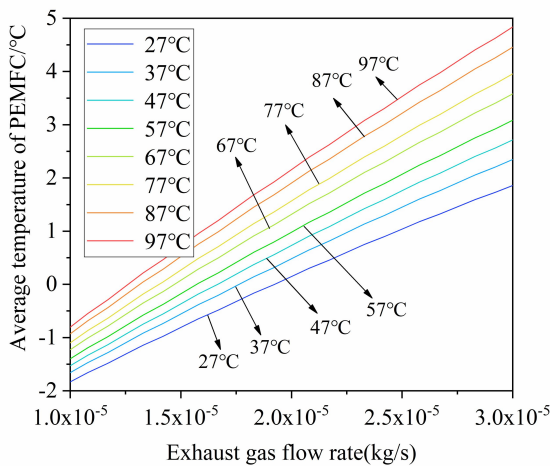
The results show that the standard deviation of PEMFC temperature is affected by both exhaust gas temperature and flow rate. When the exhaust gas temperature and flow rate are higher or lower, the effect on the standard deviation of PEMFC temperature is more obvious. The range of influence at high values of both exhaust gas temperature and flow rate is greater than at low values. The PEMFC temperature is mainly affected by exhaust gas flow rate, and exhaust gas temperature only has a certain influence on PEMFC temperature when the exhaust gas flow rate is high. Therefore, the influence of the exhaust gas temperature on the PEMFC temperature is not as strong as the exhaust gas flow rate.

The -30 °C input parameters and PEMFC temperature

standard deviation and temperature in 2D slice diagram as shown in Figure 3. The results show that the temperature of PEMFC is not lower than 0 °C, and the standard deviation of temperature is not more than 3 °C, and the exhaust gas flow rate is controlled between 1.26×10^{-5} kg/s and 2.08×10^{-5} kg/s. The optimization target value range is set as, the PEMFC temperature is not less than 0 °C, and the temperature standard deviation is not more than 3 °C, and the optimal preheating exhaust gas temperature and flow control parameters are determined to be 28 °C and 1.96×10^{-5} kg/s, respectively. At this time, the minimum temperature standard deviation is 2.9768, and the optimal premixed gas flow corresponding to the exhaust gas temperature is 1.1049×10^{-4} kg/s.



(a) 2D slice plot of exhaust gas temperature and flow rate and standard deviation of PEMFC temperature

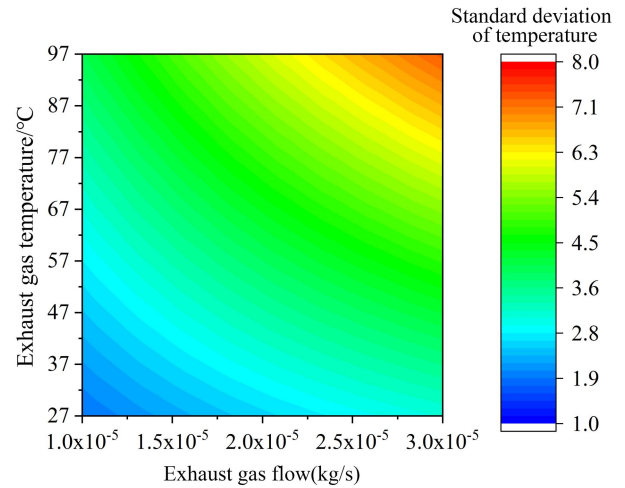


(b) 2D slice plot of exhaust gas temperature and flow rate versus PEMFC temperature

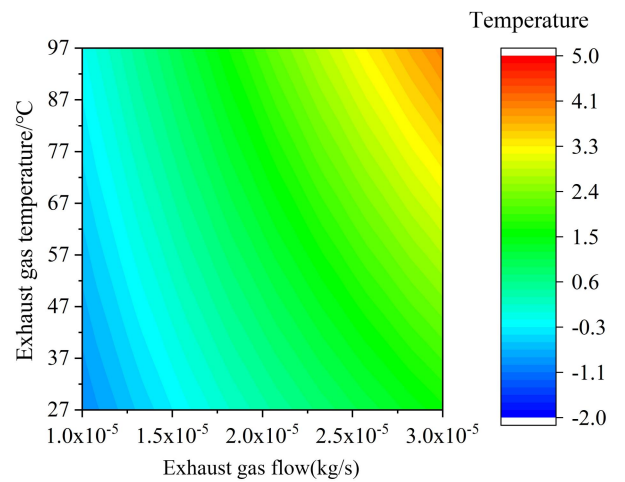
Fig. 3. -30 °C input parameters with PEMFC temperature standard deviation and temperature 2D

The -20 °C input parameters with the preheating exhaust gas temperature and flow rate are plotted against the PEMFC temperature standard deviation and temperature in the Z-axis projection map as shown in Figure 4. The standard deviation of PEMFC temperature is affected by both exhaust gas temperature and flow rate. The influence of exhaust gas

temperature and flow rate on the standard deviation of PEMFC temperature is basically consistent with that of -30 °C. However, the range of influence when the exhaust gas temperature and flow rate are high gradually decreases, and the range of influence when both are low gradually expands. The PEMFC temperature is mainly affected by the exhaust gas flow, and the influence law of the exhaust gas temperature is basically consistent with that of -30 °C. However, compared with -30 °C, the influence of exhaust gas temperature on PEMFC temperature is reduced.



(a) The standard deviation map of exhaust gas temperature and flow rate and PEMFC temperature

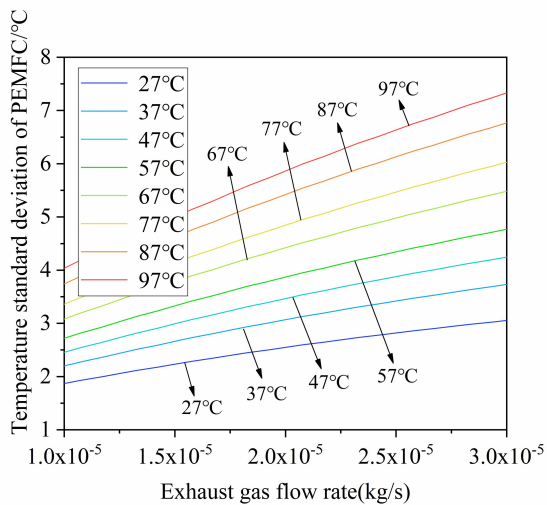


(b) Exhaust gas temperature and flow map with PEMFC temperature

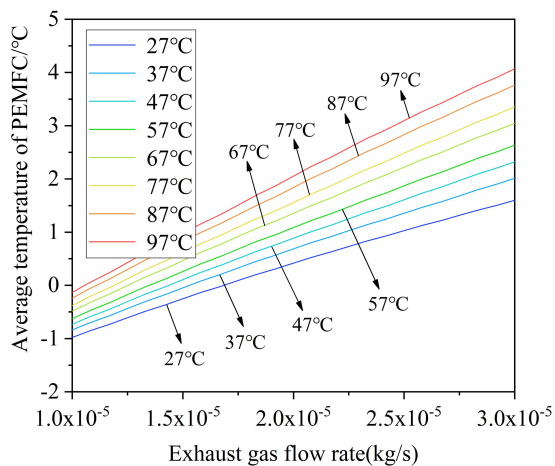
Fig. 4. -20 °C input parameters and PEMFC temperature standard deviation and temperature are projected on the Z-axis

The -20 °C input parameters are plotted against the PEMFC temperature standard deviation and temperature in 2D slices as shown in Figure 5. The results show that when the PEMFC temperature is not less than 0 °C and the temperature standard deviation is not more than 2.45 °C, the exhaust gas flow should be controlled between 1.06×10^{-5} kg/s and 1.85×10^{-5} kg/s. The value range of the optimization target is set as follows: PEMFC temperature is not less than 0 °C and temperature standard deviation is not more than 2.45 °C, and the optimal preheating exhaust temperature and flow rate control parameters are determined to be 27.91 °C and

1.7×10^{-5} kg/s, respectively. At this time, the minimum temperature standard deviation is 2.40347 °C, and the optimal premixed gas flow corresponding to the exhaust gas temperature is 1.1014×10^{-4} kg/s.



(a) 2D slice plot of exhaust gas temperature and flow rate and standard deviation of PEMFC temperature



(b) 2D slice plot of exhaust gas temperature and flow rate versus PEMFC temperature

Fig. 5. -20 °C input parameters with PEMFC temperature standard deviation and temperature 2D slice

Similarly, the optimization results of input and output parameters at -10 °C can be obtained. The warm-up time is set to 20 s, and the input parameter boundary condition setting remains the same as before. Compared with -20 °C, the influence range when the exhaust gas temperature and flow rate are high is constantly narrowing, and the influence range when the temperature and flow rate are low continue to expand. The PEMFC temperature is also affected by both the exhaust gas temperature and flow rate. However, only when the exhaust gas temperature and flow rate are high, can it have a significant effect on the PEMFC temperature. The PEMFC temperature is not less than 0 °C and the standard deviation of temperature is not more than 1.4 °C, and the optimum preheating exhaust gas temperature and flow control parameters are determined to be 27 °C and 1×10^{-5} kg/s, respectively. At this time, the minimum temperature

standard deviation is 1.3606 °C, and the optimal premixed gas flow corresponding to the exhaust gas temperature is 1.0656×10^{-4} kg/s.

IV. DESIGN OF LOW-TEMPERATURE COLD-START CONTROL STRATEGY FOR PROTON EXCHANGE MEMBRANE FUEL CELL

When the PEMFC stack is started at constant pressure and low temperature below the freezing point, the preheating exhaust gas is passed into the flow channel together with the reaction gas, and the heat carried by the external heat source and the heat released by the electrochemical reaction heat the stack together. When the temperature of the stack rises above freezing point, the external auxiliary preheating is stopped. The preheating exhaust gas temperature and flow rate at -10 °C are 27 °C and 1×10^{-5} kg/s, respectively. The preheating exhaust gas temperature and flow rate at -20 °C are 27.91 °C and 1.7×10^{-5} kg/s, respectively. The preheating exhaust gas temperature and flow rate at -30 °C are 28 °C and 1.96×10^{-5} kg/s, respectively. Hydrogen volume fraction of the preheating exhaust gas in the preheating exhaust gas was less than 1 % in all the above three operating conditions. Therefore, additional hydrogen is supplied to the anode and the hydrogen volume fraction is controlled to be less than 4 %.

Based on the above analysis, this paper designs a low-temperature start-up strategy for PEMFC reactors with auxiliary preheating under -10 °C, -20 °C and -30 °C operating conditions, as shown in Figures 6, 7 and 8. In the figure, F_{purge} , F_{H_2} , F_{gas} and F_p are the purge flow rate, anode hydrogen flow rate, preheating exhaust gas flow rate, and premixed gas flow rate, respectively. T_{purge} , T_{gas} , T_e and T are purge temperature, preheating exhaust gas temperature, ambient temperature, and stack temperature, respectively. t_{purge} and t_{heat} are the purge time and preheating time, respectively. K_m is the absolute value of the rate of change of water content in the membrane. In the process of low temperature start-up, when the flow channel and porous medium internal icing will block the reaction gas transmission channel, making the reaction gas pressure drop become larger, so the pressure drop is an important detection parameter in the process of low temperature startup of PEMFC. Therefore, in this paper, the reaction gas pressure drop is used as a sign to reflect whether the water inside the cell is iced or not. The temperature is monitored by setting up monitoring points, with the end face of the anode of the first monolithic PEMFC as the starting point and the end face of the cathode of the third monolithic PEMFC as the end point, and 11 monitoring points are set up sequentially in the centre of the end face. Then, one monitoring point is set in the inlet direction and one in the outlet direction of the end face, and so on for a total of 33 monitoring points. The average value of three monitoring points on the same plane is used to characterize the temperature value of the plane, and finally the average temperature of 13 planes is used to characterize the temperature of the PEMFC stack.

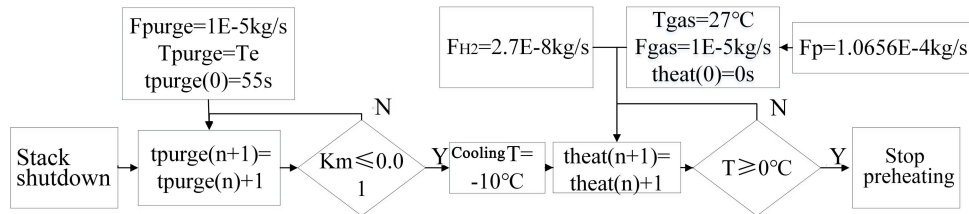


Fig. 6. Low temperature startup strategy flow for auxiliary preheating of PEMFC stack at -10 °C

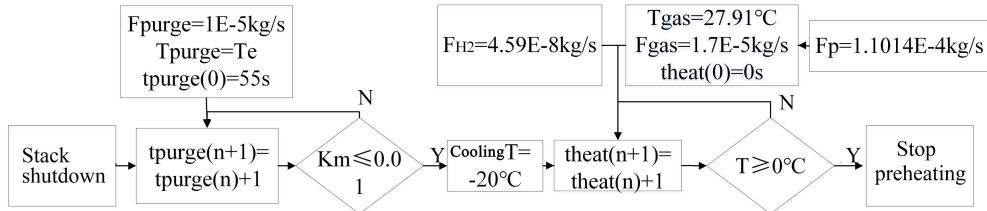


Fig. 7. Low temperature startup strategy flow for auxiliary preheating of PEMFC stack at -20 °C

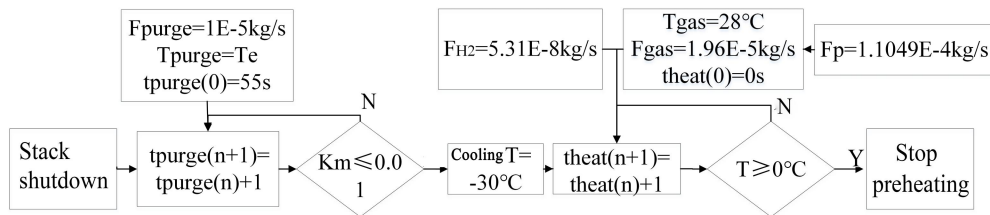


Fig. 8. Low temperature startup strategy flow for auxiliary preheating of PEMFC stack at -30 °C

V. ANALYSIS OF LOW TEMPERATURE START-UP PERFORMANCE OF PROTON EXCHANGE MEMBRANE FUEL CELLS

The start-up performance of the PEMFC at -10 °C is given as shown in Figure 9, which specifically includes the temperature, cathode pressure drop, and the average ice volume fraction of the cathode catalytic layer versus time curve. The results show that when the start-up temperature is -10 °C, the temperature of the stack can reach above the freezing point at about 18 s. The rate of temperature rise is higher than the previous unassisted low temperature start and exhaust gas preheating only. When the temperature of the stack is below the freezing point, the cathode pressure drop of the PEMFC rises rapidly due to the fact that the water generated by the electrochemical reaction at this time freezes and clogs up in the porous medium.

When the temperature of the stack rises above the freezing point, the PEMFC cathode pressure drop begins to decrease, this is because at this time the ice begins to melt, and the ice located in the porous medium melts into water, which diffuses into the flow channel and is gradually blown away by the gas. The PEMFC-1 cathode pressure drop is the largest and the PEMFC-2 cathode pressure drop is the smallest. This is caused by the maximum flow at the entrance of PEMFC-1 as well as the icing. PEMFC-2 has a faster temperature rise, so the ice starts to melt the earliest and the cathode pressure drop is the smallest. Compared with the unassisted cryostart process, the freezing rate and ice volume fraction are lower at this time because the PEMFC temperature rise rate is higher at this time, which inhibits ice formation.

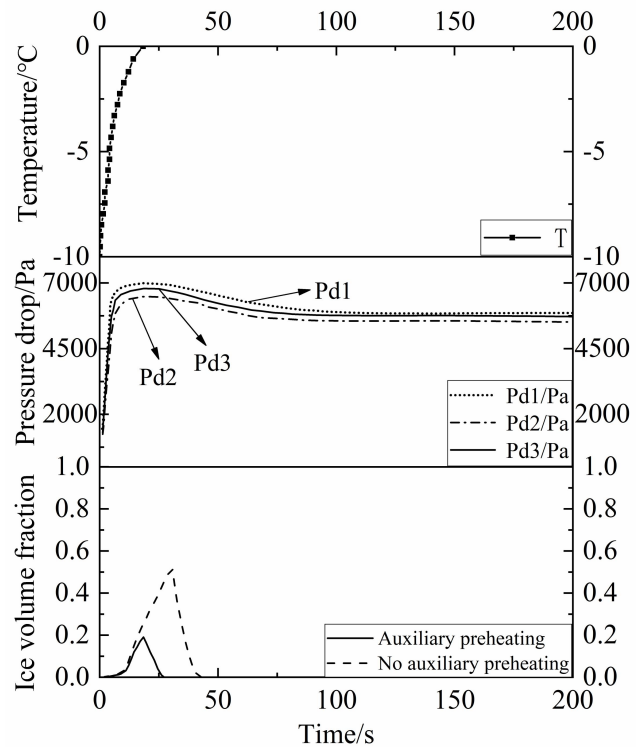


Fig. 9. Variation curves of temperature, cathode pressure drop and ice volume fraction in catalytic layer during -10 °C assisted low temperature start-up of reactor

The low temperature starting performance of the PEMFC stack with auxiliary preheating from -20 °C is shown in Figure 10. When the starting temperature is -20 °C, the auxiliary preheating time of the stack is about 32 seconds. When the stack temperature is below freezing point, the

cathode pressure drop of the PEMFC increases rapidly and the ice volume fraction gradually increases. As the stack temperature increases, the icing rate gradually decreases, and when the stack temperature rises above the freezing point, the cathode pressure drop of the PEMFC begins to decrease, at which point the ice begins to melt. Compared with the starting temperature of $-10\text{ }^{\circ}\text{C}$, the cathode pressure drop decreases more slowly, because the low temperature causes the ice to cover a larger area, so it takes more time to melt.

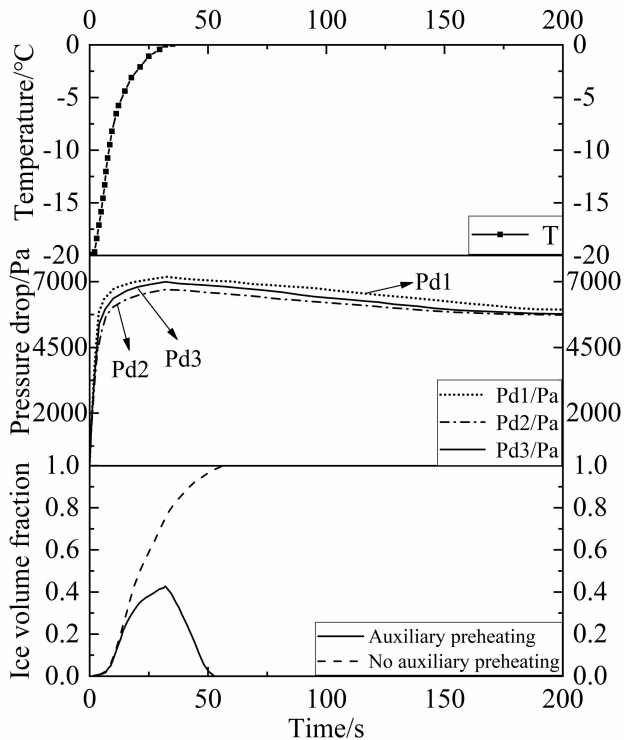


Fig. 10. Variation curves of temperature, cathode pressure drop and ice volume fraction in catalytic layer during $-20\text{ }^{\circ}\text{C}$ assisted low temperature start-up of reactor

The low-temperature start-up performance of the PEMFC stack with auxiliary preheating from $-30\text{ }^{\circ}\text{C}$ is shown in Figure 11. The required auxiliary preheating time of the stack is about 47 seconds when the startup temperature is $-30\text{ }^{\circ}\text{C}$. When the temperature of the stack is below freezing point, the PEMFC cathode pressure drop and the ice volume fraction in the catalytic layer gradually increase, but the rate of increase is lower than that of $-20\text{ }^{\circ}\text{C}$ condition. Although the freezing rate is higher at a start-up temperature of $-30\text{ }^{\circ}\text{C}$, the PEMFC stack has a weak catalyst activity at the beginning of the low-temperature start-up, producing less water and less icing. The PEMFC cathode pressure drop and catalytic layer ice volume fraction begin to decrease when the stack temperature rises above freezing point. Compared with the previous two conditions, the cathode voltage drop at this point decreases more slowly, because when the stack temperature rises above freezing and the auxiliary preheating is turned off, the electrochemical reaction becomes the only source of heat for melting the ice, and a longer low-temperature startup time results in more ice in the battery, so the cathode voltage drop at this point decreases more slowly.

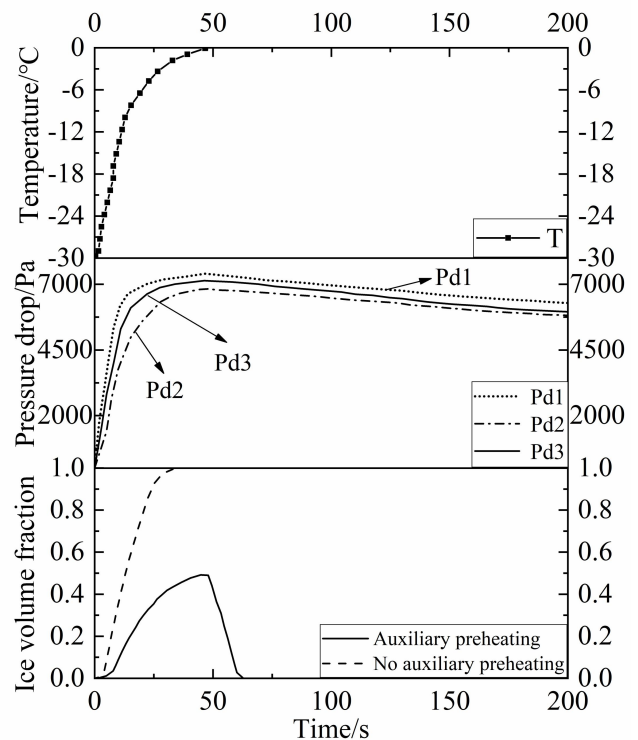


Fig. 11. Variation curves of temperature, cathode pressure drop and ice volume fraction in catalytic layer during $-30\text{ }^{\circ}\text{C}$ assisted low temperature start-up of reactor

VI. CONCLUSION

(1) The preheating time is 50 s at $-30\text{ }^{\circ}\text{C}$, and the optimal preheating exhaust gas temperature and flow rate operating parameters are $28\text{ }^{\circ}\text{C}$ and $1.96 \times 10^{-5}\text{ kg/s}$ respectively under the optimization constraints. The preheating time is 35 s at $-20\text{ }^{\circ}\text{C}$, and the optimal preheating exhaust gas temperature and flow rate operating parameters are $27.91\text{ }^{\circ}\text{C}$ and $1.7 \times 10^{-5}\text{ kg/s}$ respectively under the optimization constraints. The preheating time is 20 s at $-10\text{ }^{\circ}\text{C}$, and the optimal preheating exhaust gas temperature and flow rate operating parameters are $27\text{ }^{\circ}\text{C}$ and $1 \times 10^{-5}\text{ kg/s}$ respectively under the optimization constraints.

(2) When the PEMFC stack is started from different starting temperatures, the lower the starting temperature, the lower the temperature rise rate of the stack, the longer the auxiliary preheating time, and the more fuel consumption. When the starting temperature is $-10\text{ }^{\circ}\text{C}$, the time required for the low temperature starting process with auxiliary preheating is 18 s, which is 43 % less than that of the low temperature starting process without auxiliary preheating. When the starting temperatures are $-20\text{ }^{\circ}\text{C}$ and $-30\text{ }^{\circ}\text{C}$, the time required for low temperature starting of the stack assisted preheating is 32 s and 47 s, respectively.

(3) By comparing the change law of the cathodic pressure drop of each PEMFC during the low temperature start-up process of auxiliary preheating at different starting temperatures, it is found that the cathodic pressure drop of PEMFC-2 is smaller than that of other PEMFC, which indicates that the temperature rise of PEMFC-2 is faster and the internal ice is less $10\text{ }^{\circ}\text{C}$.

REFERENCES

- [1] Rajendran N, Baskaran S, Natarajan R. Carbon-free hydrogen and bioenergy production through integrated carbon capture and storage technology for achieving sustainable and circular economy– A review[J]. *Fuel*, 2023, 342.
- [2] Wiloso E, Heijungs R, Huppes G. Effect of biogenic carbon inventory on the life cycle assessment of bioenergy: challenges to the neutrality assumption[J]. *Journal of Cleaner Production*, 2016, 125.
- [3] Q.L. Y, C.X. H, J. S. A passive thermal management system with thermally enhanced water adsorbents for lithium-ion batteries powering electric vehicles[J]. *Applied Thermal Engineering*, 2022, 207.
- [4] Huang Y, Tang Y, Yuan W. Challenges and recent progress in thermal management with heat pipes for lithium-ion power batteries in electric vehicles[J]. *Science China Technological Sciences*, 2021, 64(5).
- [5] Dong T, Zhen Z, Lun H. Prediction of cold start emissions for hybrid electric vehicles based on genetic algorithms and neural networks[J]. *Journal of Cleaner Production*, 2023, 420.
- [6] A. C R. (Invited) Automotive Proton Exchange Membrane Fuel Cells Subzero Performance[J]. *Electrochemical Society Meeting Abstracts*, 2021, MA2021-02(37).
- [7] Landi G, Benedetto D A, Lisi L. Two-Stage Strategy for CO Removal from H₂-Rich Streams over (Nano-) CuO/CeO₂ Structured Catalyst at Low Temperature[J]. *Applied Sciences*, 2018, 8(5).
- [8] Li L, Wang S, Yue L. Cold-start icing characteristics of proton-exchange membrane fuel cells[J]. *International Journal of Hydrogen Energy*, 2019, 44(23).
- [9] Lin R, Weng Y, Li Y. Internal behavior of segmented fuel cell during cold start[J]. *International Journal of Hydrogen Energy*, 2014, 39(28).
- [10] Le L, Pu H, Peng H. Numerical Research on the Cold Start-up Strategy of a PEMFC Stack from -30 °C[J]. *Journal of Thermal Science*, 2022, 32(3).
- [11] Tom G, Thomas J. Assisted cold start of a PEMFC with a thermochemical preheater: A numerical study[J]. *Applied Energy*, 2023, 331.
- [12] Rui L, Di Z, Shunbo L. Experimental validation for enhancement of PEMFC cold start performance: Based on the optimization of micro porous layer[J]. *Applied Energy*, 2021, 300.